A Novel Location Method for Interline Power Flow Controllers Based on Entropy Theory

Qiuyu Li, Baohong Li, Qin Jiang, Tianqi Liu, Yin Yue, and Yingmin Zhang

***Abstract*—As one of the new generation flexible AC transmission systems (FACTS) devices, the interline power flow controller (IPFC) has the significant advantage of simultaneously regulating the power flow of multiple lines. Nevertheless, how to choose the appropriate location for the IPFC converters has not been discussed thoroughly. To solve this problem, this paper proposes a novel location method for IPFC using entropy theory. To clarify IPFC's impact on system power flow, its operation mechanism and control strategies of different types of serial converters are discussed. Subsequently, to clarify the system power flow characteristic suitable for device location analysis, the entropy concept is introduced. In this process, the power flow distribution entropy index is used as an optimization index. Using this index as a foundation, the power flow transfer entropy index is also generated and proposed for the IPFC location determination study. Finally, electro-mechanical electromagnetic hybrid simulations based on ADPSS are implemented for validation. These are tested in a practical power grid with over 800 nodes. A modular multilevel converter (MMC)-based IPFC electromagnetic model is also established for precise verification. The results show that the proposed method can quickly and efficiently complete optimized IPFC location and support IPFC to determine an optimal adjustment in the N-1 fault cases.**

***Index Terms*—Flexible alternative current transmission systems, interline power flow controller, modular multilevel converter, optimized location method, power flow transfer entropy.**

I. Introduction

The modern power system is currently experiencing a rapid surge in electricity demand, resulting in increased pressure on long-distance power transmission, transmission lines approaching their thermal limits, and increased risks of voltage deviation [1], [2]. Consequently, the security and stability of the system's operation may be affected. Therefore, it is imperative to ensure that the system operates safely within an economical range without compromising the load demand. One solution is to control power flow within the thermal stability limit of the grid to enable efficient transmission at higher power levels. Because of factors such as geographical and economic load distribution, power flow distribution in power systems is often uneven, resulting in overloaded load centers and underutilized lines. These pose risks to system transmission. Disturbances in load centers can easily lead to chain failures in other lines, resulting in system instability. Traditional methods like adding new transmission lines or infrastructure upgrades are expensive, time-consuming, and often infeasible because of practical constraints.

Flexible AC transmission systems (FACTS), using high-power semiconductor devices for fast controllability, play a significant role in enhancing the performance of AC transmission systems. FACTS have been studied and applied in power flow control, voltage support, reactive power compensation, and low-frequency oscillation damping [3]–[6]. FACTS can contribute to improved operational efficiency and utilization of existing transmission facilities, making them an important focus in the development of modern power systems [7], [8].

The interline power flow controller (IPFC), as a third-generation FACTS device [9], offers greater flexibility and versatility than other devices that can only control a single system parameter. IPFC can simultaneously compensate multiple lines, enabling independent control of active and reactive power [10]–[12]. However, aside from effective control strategies, the appropriate placement of IPFC converters within the grid is also vital for achieving optimal performance.

Several studies have addressed these issues using different techniques and methods. The optimal power flow (OPF) algorithm is commonly used for evaluating the operation of FACTS devices [13], [14]. In [15], a dual-layer optimization model for the placement of voltage source converters (VSCs) and phase shifting transformers (PST) is proposed to address the intermittent and insufficient long-distance transmission capacity of grid-connected wind power generation. The model aims to minimize investment costs and uses a reconstruction decomposition algorithm to reduce wind

Received: June 20, 2023
Accepted: December 1, 2023
Published Online: May 1, 2024
Baohong Li (corresponding author) is with the School of Electrical Engineering, Sichuan University, Chengdu 610065, China (scu_lbh@163.com).
DOI: 10.23919/PCMP.2023.000504

abandonment. Reference [16] presents a mathematical planning method based on the branch and bound (B&B) algorithm, which considers the thermal limit of transmission lines and determines the optimal configuration of thyristor-controlled series compensators (TCSCs) in the transmission system with the maximum load as the objective. In [17], different load demand scenarios, such as peak and minimum demands, are considered, and Pareto optimization is employed for FACTS placement to provide corresponding decision schemes.

In recent years, evolving and improving meta-heuristic optimization methods have become important tools for addressing these problems because of their efficiency in handling multi-modal, highly constrained, multi-objective, and discrete problems [18]. Among these methods, population-based artificial intelligence techniques like particle swarm optimization have been widely used in various scenarios, often combined with other techniques [19]–[22]. Evolutionary artificial intelligence techniques, including differential evolution and genetic algorithms, have also gained in popularity [23]–[25]. In [26], an improved hybrid moth-flame optimization algorithm is used to locate TCSC and SVC to reduce both costs and active power losses, enhancing the algorithm's convergence by eliminating the worst agent. In [27], a multi-objective nondominated sorting (MNS) genetic algorithm is used to determine the unified power flow controller (UPFC) location considering the uncertainty of wind power generation probability characteristics, so as to improve system predictability and reduce active losses. Reference [28] proposes a novel heuristic algorithm for large-scale transmission systems, one that considers operational costs and various load scenarios for FACTS configuration, ensuring feasible optimal solutions across different scenarios. In [29], aiming at reducing IPFC active power losses, the data clustering method is introduced into the multi-objective particle swarm algorithm to improve the convergence speed of the algorithm. Reference [30] proposes a method for optimal placement of IPFC based on disparity line utilization factor (DLUF) and firefly algorithm-based optimal tuning for a multi-objective function to control the congestion in transmission lines. However, because of the stochastic nature of the meta-heuristic algorithms, optimal solutions cannot be guaranteed, and the solutions obtained may be conservative.

Most existing methods for locating IPFC are primarily based on straightforward indicators such as load ratios, voltage deviations, and investment costs. These methods often overlook comprehensive consideration of the system's flow distribution characteristics. Employing intelligent optimization algorithms for the placement of IPFC can present the challenge of getting trapped in local optima if the iteration parameters are not adequately configured. In contrast to other FACTS devices such as the static synchronous compensator (STATCOM) and the static synchronous series compensator (SSSC), a significant advantage of IPFC is its ability to independently control multiple line parameters. Therefore, the aforementioned configuration methods for other types of FACTS devices cannot be directly applied to IPFC, because more objectives need to be considered for optimization.

To solve the location optimization problem for IPFC, this paper proposes an IPFC placement method based on the system power flow transfer entropy index (PFTEI), which takes into account the system power flow shifting characteristics and the global optimality of the scheme, serving as a backstop for intricate grid operations. The approach mitigates the effect of flow transfers, reinforces the weaker links in the network, and ultimately reduces the risk of cascading failure by rationally configuring the IPFC. The novelty of the paper can be summarized as follows:

1) The power flow distribution entropy index is used to clarify the system's power flow characteristics in steady operation. The IPFC's impacts on the system are also studied through the power flow distribution entropy index, which can evaluate the system efficiently.

2) Referring to the concept of vulnerability analysis, the novel power flow transfer entropy index is derived from the existing power flow entropy to assess the vulnerability of lines, so as to obtain a globally optimal solution. In addition, considering the varied operational situations, the *N*-1 fault scenarios are also considered when deciding the location of IPFC.

3) To verify the proposed method, the electromechanical electromagnetic hybrid models based on ADPSS are established, and a practical large-scale power grid is also used for simulations, to prove the methods' applicability and practicality.

The rest of the paper is organized as follows: Section II introduces the basic structure and operation mechanism of IPFC, while Section III describes the entropy theory and the index that is used. Section IV studies the location method for IPFC through the entropy concept, and Section V verifies the proposed method through simulation. Section VI concludes the paper.

II. The Structure and Mechanism of IPFC

A. Structure of IPFC

An IPFC consists of multiple parallel back-to-back VSCs, connected in parallel onto a common DC bus, enabling active power exchange between the converters, as illustrated in Fig. 1. On the AC side, the VSCs are connected in series with the system buses through coupling transformers, injecting series voltages with controllable amplitude and phase angle to control power flows.

Among these converters, one converter is designated as the auxiliary control converter, while the others serve

as the main control converters. The auxiliary control converter is typically installed on a bus with a relatively low power flow. Its role is to maintain the stability of the common DC bus voltage, as well as to control the active or reactive power in the connected line. The main control converters are usually installed on buses with heavy power flow, so they can control the active and reactive power in the lines based on the setpoints. This enables the adjustment of the system power flow distribution to alleviate problems arising from line overloads and uneven power flow distribution.

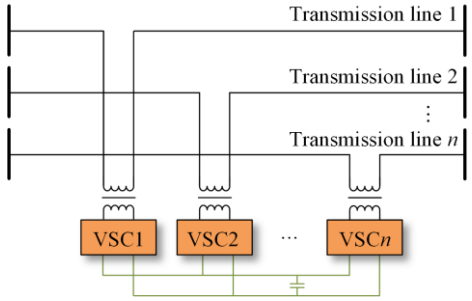

Fig. 1. Structure of IPFC.

The IPFC converters maintain a dynamic balance of active power among themselves, maintaining a stable common DC bus voltage. As a result, their operation is bounded by the restriction of conserving internal active power. Therefore, in the context of the entire system, IPFC neither generates nor consumes any active power.

B. Controller Strategy and Operation Mechanism of IPFC Converters

The modular multilevel converter (MMC) is a type of VSC that uses multiple cascaded insulate-gate bipolar transistor (IGBT) submodules. The structure of the MMC is shown in Fig. 2. This configuration allows a low operating frequency and voltage of the switching devices, while producing output voltage waveforms that closely resemble sinusoidal waves. In practical operation, each MMC in the IPFC selects its own control objectives for active and reactive power. The active power control objectives encompass the DC-side voltage and active power output, while the reactive power control objectives involve the AC-side bus voltage amplitude and reactive power output.

To facilitate controller design, the complex frequency domain form of the fundamental frequency dynamic equation of MMC in the *dq* rotating coordinate system is derived through coordinate and Laplace transformation, given as:

$$\begin{cases}\left[\dfrac{R_0}{2}+\left(L_{\mathrm{ac}}+\dfrac{L_0}{2}\right)s\right]i_{\mathrm{v}d}(s)=-u_{\mathrm{s}d}(s)+u_{\mathrm{diff}\,d}(s)+\omega L i_{\mathrm{v}q}(s)\\ \left[\dfrac{R_0}{2}+\left(L_{\mathrm{ac}}+\dfrac{L_0}{2}\right)s\right]i_{\mathrm{v}q}(s)=-u_{\mathrm{s}q}(s)+u_{\mathrm{diff}\,q}(s)-\omega L i_{\mathrm{v}d}(s)\end{cases} \tag{1}$$

where L_0 and R_0 are the inductance and equivalent resistance of the bridge arm, respectively, while L_{ac} is the equivalent inductance between the converter AC terminal and the AC system equivalent power source. $i_{\mathrm{v}d}$ and $i_{\mathrm{v}q}$ are the *dq*-axis components of the MMC output current, $u_{\mathrm{s}d}$ and $u_{\mathrm{s}q}$ are the *dq*-axis components of the AC system voltage, whereas $u_{\mathrm{diff}\,d}$ and $u_{\mathrm{diff}\,q}$ are the *dq*-axis components of the bridge arm differential mode voltage.

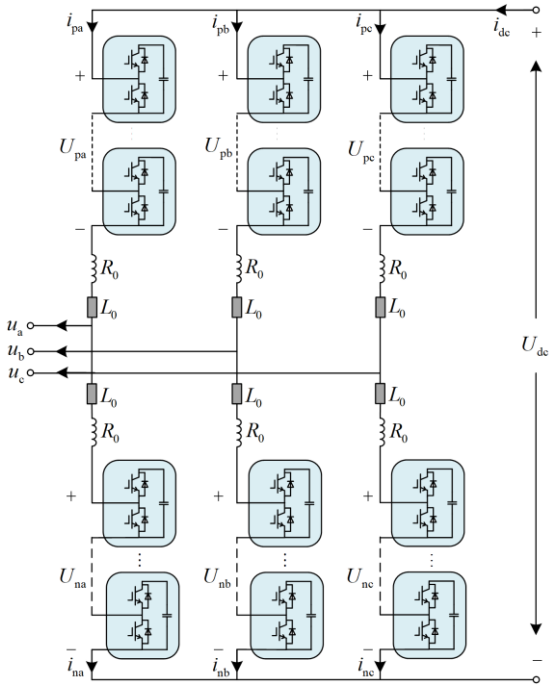

Fig. 2. Structure of modular multilevel converter.

As the MMC output current depends on the system voltage and bridge arm voltage, it is necessary to establish the transfer function between $i_{\mathrm{v}d}$, $i_{\mathrm{v}q}$, $u_{\mathrm{diff}\,d}$, and $u_{\mathrm{diff}\,q}$. Constructing the control variables V_d and V_q as:

$$\begin{cases}V_d(s)=-u_{\mathrm{s}d}(s)+u_{\mathrm{diff}\,d}(s)+\omega\left(L_{\mathrm{ac}}+\dfrac{L_0}{2}\right)i_{\mathrm{v}q}(s)\\ V_q(s)=-u_{\mathrm{s}q}(s)+u_{\mathrm{diff}\,q}(s)-\omega\left(L_{\mathrm{ac}}+\dfrac{L_0}{2}\right)i_{\mathrm{v}d}(s)\end{cases} \tag{2}$$

The current controller can be obtained by introducing a PI control loop while decoupling the *dq*-axis current by substituting V_d and V_q into the MMC mathematical model, as shown in the blue part in Fig. 3. As seen, the current controller gives the setpoints of $u_{\mathrm{diff}\,d}$ and $u_{\mathrm{diff}\,q}$, which are then used to calculate the corresponding bridge arm voltage modulation waveform for controlling the waveform output of the MMC submodules. The setpoints of $i_{\mathrm{v}d}$ and $i_{\mathrm{v}q}$ are calculated by the power controller. In the steady-state, the instantaneous power

output of the IPFC to the AC system is determined as:

$$p_s = \frac{3}{2} u_{sd} i_{vd} \tag{3}$$

$$q_s = -\frac{3}{2} u_{sd} i_{vq} \tag{4}$$

From (3) and (4), the reference values for the *dq* currents can be obtained from the provided reference active and reactive power values. To eliminate steady-state errors, PI control loops are added to control active and reactive power. In cases where the control objective is the DC-side voltage U_{dc}, it is achieved through a PI controller, which adjusts the *d*-axis current to regulate the active power absorbed from the AC side by the MMC. The controller block diagram of the MMC is shown in Fig. 3. Generally, to control the power of the target line to a specified value and to achieve the desired power flow distribution in the system, the control objectives of the main control converter are the active and reactive power output values $P_{ij\,\mathrm{ref}}$ and $Q_{ij\,\mathrm{ref}}$. To maintain a constant DC bus voltage, the control objectives of the auxiliary control converter are the DC-side voltage U_{dc} and the reactive power output $Q_{ik\,\mathrm{ref}}$.

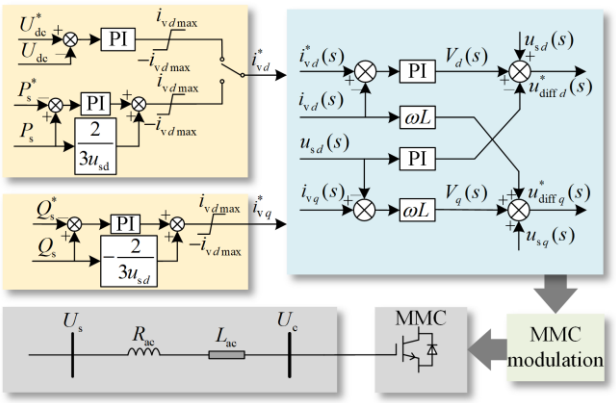

Fig. 3. Control system diagram of MMC.

III. The Entropy Concept and Power Flow Distribution Entropy Index

A. Entropy Theory

Entropy reflects the evolution of the degree of orderliness of a natural phenomenon and is widely used in the description of system uncertainty and stability. Entropy is used in physics to describe the degree of disorder in the motion of molecules within a system, whereas information entropy is used to describe the information uncertainty of discrete systems [31].

The system entropy is defined as:

$$H = -M \sum_{i=1}^{s} P(X_i) \ln P(X_i) \tag{5}$$

where M is a constant; s is the number of states of the system; and $P(X_i)$ is the probability of the state X_i occurring.

Information entropy is a probabilistic description to judge the certainty of the state of the system. When the system is in a unique state, the degree of order of the system is the highest, and the entropy of the system is the minimum 0. When the system is in multiple states with equal probability, the degree of order of the system is the lowest, and the entropy of the system is the maximum. For a generalized complex system, entropy can be used as a measure of the disorder and randomness of the distribution state. Because of its unique and general principles, entropy has been widely applied in the measurement of disorder in complex systems [32], [33].

Choosing the constant M as 1, if the system has only one state with a probability of 1, the system operates in the most ordered state with an entropy value of 0. If the system has s operating states with the same probability of occurrence, the system operates in the most chaotic state with an entropy value of ln(s).

B. Power Flow Distribution Entropy Index

The electric power system maintains dynamic equilibrium between the generation and consumption of internal energy. Disturbances introduce energy-related effects that drive the system towards a state of disorder, leading to a redistribution of power flows. Consequently, the concept of entropy can be introduced to reflect the various characteristics and changes within the system's power flow distribution. The power flow distribution entropy of a power system can describe the internal energy distribution law of the system in a certain state, measure the stability of the system, and characterize the influence of the disordered distribution of power flow on grid chain faults.

We define the load rate of system line k as:

$$\beta_k = \frac{P_k}{P_{k\max}} \tag{6}$$

where P_k is the active power of line k; and $P_{k\max}$ is the thermal stability limit power of line k.

Power flow in the line can be bidirectional, but we consider the power flowing out from the i-side bus in this paper. When the system experiences an inadequate distribution of power flows, there are significant variations in the load rate of the lines, ultimately leading to a low degree of load rate balance. During disturbances, lines with high load rates are at risk of experiencing current overtripping and cascading overload trip incidents, while lines with low load rates remain underutilized.

Given the load rate constant sequence $E = [0, \mathrm{e}, 2\mathrm{e}, \cdots, q\mathrm{e}]$, where $q\mathrm{e} = 1$, and in this section, e is taken as 10%. Z_m is used to represent the number of lines whose load rate is in the interval [me, (m+1)e]. Then the probability P_m of the line being in the interval [me, (m+1)e] is given as:

$$P_m = \frac{Z_m}{Z} \tag{7}$$

We define the average system load ratio as:

$$\bar{\beta} = \frac{1}{Z}\sum_{k=1}^{Z}\beta_k \tag{8}$$

where Z is the number of bus routes in the system. The average load rate of the system is an important factor affecting the propagation of cascading failures in the power grid, as the system is more likely to experience non-fault line overloads after a fault when the average load rate is high.

The power flow distribution entropy index (PFDEI) of the system is defined as:

$$\text{PFDEI} = -\sum_{m=0}^{q}\overline{\beta_m}P_m \ln P_m \tag{9}$$

where $\overline{\beta_m} = \frac{1}{Z_m}\sum_{j=1}^{Z_m}\beta_{mj}$ is the average load rate of all lines in the interval [me, (m+1)e]; and β_{mj} is the load rate of the line j in the [me, (m+1)e] interval of load rates.

PFDEI characterizes the steady-state load rate distribution in the system. A larger PFDEI indicates a more uneven distribution of load rates among the transmission lines. This reduces the safety of the power system. IPFC can control the power flow of multiple transmission lines simultaneously, thereby mitigating the problems of transmission line overload and uneven power flow distribution. By calculating the power flow distribution entropy index and determining the optimal IPFC control instructions, the load rate distribution of the system can be made more uniform, resulting in a higher level of system security and more efficient control.

IV. IPFC Converter Location Method Based on Entropy Index

A. Power Flow Transfer Entropy Index

The primary principle behind the existing power flow entropy is to reflect the severity of the impact caused by a line outage. However, given the inherent uncertainty surrounding the precise location of a line fault, simply reducing the likelihood of faults on a few lines is insufficient for improving the overall flow distribution of the system. Hence, this paper proposes an enhanced calculation method for power flow transfer entropy. The flow transfer ratio is defined as:

$$\text{PFTEI}_i = -\sum_{\substack{k=1\\k\neq i}}^{n}\beta_{ik}\eta_{ik}\ln\eta_{ik} \tag{10}$$

where ΔP_{ik} represents the increase in active power allocated to line i when line k is disconnected; and ΔP_k represents the decrease in active power increment when line k is disconnected.

As the magnitude of load transfer remains constant, lines with higher load ratios face increased risk of overloading. Hence, line load ratios are employed to perform a weighted calculation of line flow transfer proportions. The refined expression for the power flow transfer entropy is given as:

$$\text{PFTEI}_i = -\sum_{\substack{k=1\\k\neq i}}^{n}\beta_{ik}\eta_{ik}\ln\eta_{ik} \tag{11}$$

The PFTEI of a line represents the probability distribution of the load rate state after power flow transfer occurs in the system. The magnitude of the power flow transfer entropy index of a line indicates the impact of other line disconnections on the line. A higher power flow transfer entropy index means that the line is carrying a large share of power flow transfer because of system line faults, signifying a more significant impact and variability in load rate resulting from power flow transfer. By pre-calculating the power flow transfer entropy index, the optimal IPFC installation location can be selected along the line with the highest index value. This allows the IPFC to promptly control heavily loaded lines following system line faults, thereby maximizing the improvement of uneven power flow distribution resulting from flow transfer, and fully utilizing the available transmission line capacity.

B. Location Determination Process

Based on the power flow transfer entropy index and power flow distribution entropy index theories proposed above, the process for determining the location and capacity of the IPFC is as follows:

Step 1: Calculate the initial power flow in the system without IPFC installation.

Step 2: Calculate the PFTEI of the system lines. Disconnect each line in sequence and perform a power flow calculation to determine the amount of power flow transfer to other lines caused by the disconnection. If the power flow calculation fails to converge after line k is disconnected, skip the calculation of power flow transfer entropy index for that iteration and proceed to the next power flow calculation. Repeat this process until all lines in the system have been disconnected once. For line i, substitute the load rate and power flow transfer amount for different line disconnections into (11) to calculate the PFTEI. Repeat this process for other lines.

Step 3: Sort the PFTEI values of the lines in the system in descending order.

Step 4: Determine the installation location for the main control converter. Based on the sorted PFTEI values, select the line with the highest PFTEI as the main control line for installing the IPFC for power flow management.

Step 5: Determine the installation location for the auxiliary control converter. After determining the main control line, select the line with the lowest PFTEI among the lines connected to the same bus of the main control line for installing the auxiliary control converter.

Step 6: Optimize the IPFC control instructions. The

converter commands are incrementally adjusted from the lower limit value to the upper limit value in steps. After each step change, the PFDEI is calculated. Evaluating all simulation outcomes allows for the identification of the scheme with the smallest PFDEI value. This approach yields optimized commands that lead to a more balanced flow distribution within the system. The step size and range for varying the commands should be determined based on the initial flow conditions of the power grid and the thermal stability limits of the lines.

Step 7: Verify the feasibility of equipment installation. Specific verification criteria procedures are:

1) Check if the lengths of the selected transmission lines are sufficient.

2) Assess whether there is enough capacity margin in the auxiliary control line.

3) Ensure that the controlled line flows remain within permissible limits.

4) Evaluate whether the installation induces overload in other devices.

5) Confirm if the voltages of the connected buses meet operational requirements.

It is necessary to clarify that in Step 2, when load flow calculations fail to converge, the severity of the fault has surpassed the controllable range of the flexible devices. At this point, the power system cannot facilitate the stable operation of the devices. Therefore, cases where post-outage flow does not converge are excluded from the scope of PFTEI calculations. The flowchart of the process for determining the locations is shown in Fig. 4.

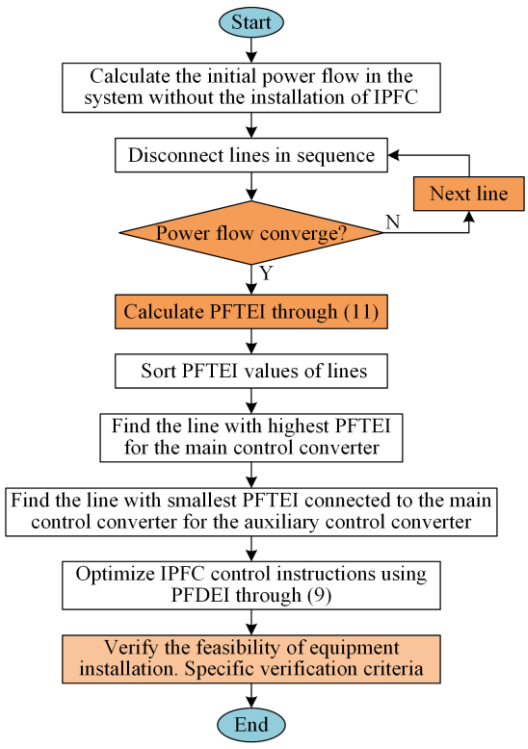

Fig. 4. Flowchart of location determination of IPFC.

V. Simulation Results

To verify the effectiveness of the proposed method, the optimal installation location and parameters of IPFC are studied for a practical power grid, and simulations are conducted on an advanced digital power system simulator (ADPSS) platform. The system comprises 881 buses and 165 generator units, and there are 268 candidate 500 kV transmission lines that can be considered for equipment allocation. Figure 5 shows the simulation topology, in which the names of the lines are determined based on the names of the sending and receiving buses. Additionally, some modifications have been applied to the data to ensure confidentiality. The simulation parameters are shown in Table I.

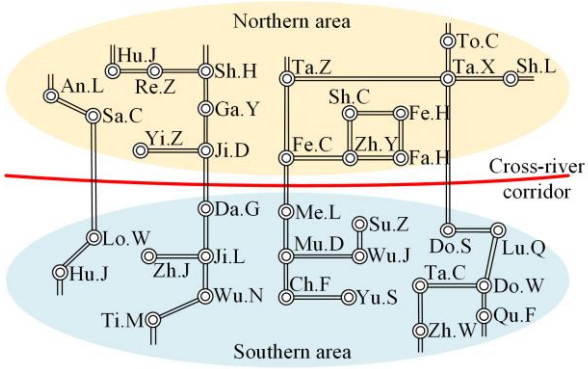

Fig. 5. Topology of the cross-river corridor in the grid.

TABLE I
Simulation Parameters

Parameter	Value
Rated voltage of the AC system	500 kV
Capacity of transformers	330 MVA
Rated voltage of the DC system	400 kV
Capacity of MMC	667 MVA
Number of sub-module on single bridge arm	30
Bridge arm inductance	80 mH
Capacitance of sub-module	2472 μF

The results of the PFTEI calculation for all lines in the system are arranged in descending order. To facilitate comparative ranking, the PFTEI values are normalized, while all the normalized PFTEI values are within the range of [0, 1]. Table II shows some top-ranked line data. From Table II, line GAD is the most affected by power flow transfer, making it the optimal installation location for the IPFC main control converter. In practice, because of geographical constraints, the distribution of offshore wind power in the region is concentrated in the northern area, while the load centers are situated in the southern region. The GAD line serves as a cross-river backbone corridor, and plays a pivotal role in the transmission capacity of the local power system. The line with the lowest PFTEI is least affected by the *N*-1 fault, providing a larger power flow control space. Among the lines connected to line GAD, the line with the smallest PFTEI value can be

used as the installation location of the auxiliary control converter. The PFTEI data for other lines connected to line GAD are shown in Table III. As seen, line YIZ has the lowest PFTEI, making it the installation location for the IPFC auxiliary converter. After placing IPFC at the proposed locations, it is then tuned for the smallest PFDEI value. Additionally, to demonstrate the superiority of the PFDEI over a single load ratio index, a simulation is conducted with IPFC installed on line FEM, which is one of the power grid interfaces. The PFTEI and active power of line FEM are 1.09 and 8, respectively. In this study, simulations are performed and analyzed for both steady-state and *N*-1 fault conditions for the two installation locations.

TABLE II
RANKING OF PFTEI CALCULATION RESULTS

Line	PFTEI	Active power without IPFC (p.u.)	Reactive power without IPFC (p.u.)
GAD	1.0000	8.9661	0.0674
YUF	0.8757	8.6549	1.7450
SUJ	0.749 79	−15.361	−0.7201
TAZ	0.7136	−3.6702	−0.3852
FED	0.6925	9.2034	0.5040
DOT	0.6637	−5.0820	−1.9145
CHJ	0.6307	−7.5349	−0.5271
TAF	0.5884	−9.8349	0.6085
TOT	0.5861	0.5901	−0.8726
DOF	0.5857	8.9531	2.2942

TABLE III
PARAMETERS OF LINES CONNECTED TO LINE GAD

Line	PFTEI	Active power without IPFC (p.u.)	Reactive power without IPFC (p.u.)
GAJ	0.0072	4.0653	0.3270
YOJ	0.8351	2.4294	0.4059
YIJ	0.0061	0.1455	0.3612
YAJ	0.0292	5.0652	0.1310

1) System Steady State

Without IPFC, the PFDEI of the system is calculated to be 1.2737 using (9). Figure 6 shows the change in PFDEI in steady-state condition with IPFC control.

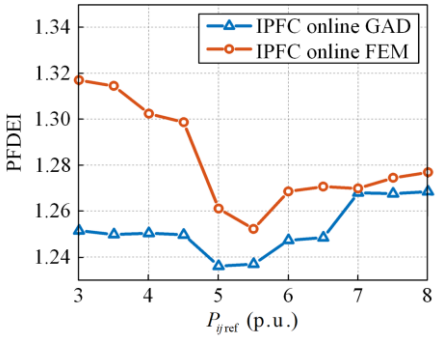

Fig. 6. The PFDEI with IPFC on different lines under the steady state.

Different power instructions for the IPFC result in varying power flow distribution and different levels of equilibrium. When the IPFC is placed on lines GAD and FEM, the system's PFDEI achieves minimum values of 1.2360 and 1.2522, respectively. This represents a reduction of 0.0377 and 0.0215, respectively, compared to the system without IPFC. The control instructions for the IPFC, when the PFDEI is at its minimum, are shown in Table IV.

TABLE IV
OPTIMAL IPFC INSTRUCTIONS AT STEADY STATE

IPFC location	$P_{ij\,\mathrm{ref}}$ (p.u.)	$Q_{ij\,\mathrm{ref}}$ (p.u.)	$Q_{ik\,\mathrm{ref}}$ (p.u.)	PFDEI
GAD	5	0.46	0.04	1.2360
FEM	5.5	1.05	1.26	1.2522

Table V presents the power flow data for several lines in different conditions. By comparing the power flows of the system before and after tuning the IPFC control instructions, a difference in the degrees of power flow regulation can be observed between the two cases. The simulation curves of the output power of the IPFC under the optimal instruction at steady state are shown in Fig. 7, while Fig. 8 compares the power distribution before and after IPFC installation on lines GAD and FEM. In both cases, the active power of the heavily loaded lines decreases, while the transmission power of the lightly loaded lines increases. For instance, with tuned IPFC on line GAD, the active power of line 3 decreases from 896 MW to 491 MW, while the transmission power of line 22 increases from 14 MW to 403 MW. With tuned IPFC on line FEM, the active power of line 8 increases from 226 MW to 558 MW, and the transmission power of line 13 increases from 408 MW to 679 MW. Compared to line FEM, the installation of IPFC on line GAD demonstrates better control on balancing power flow distribution. Also, lines in close proximity or having a tighter association with the converter exhibit more noticeable differences. In contrast, lines that are situated farther away or are not given priority have their power flows primarily dictated by line structures and load demands, reflecting smaller variances. Thus the differences before and after tuning IPFC on such lines are either negligible or minimal.

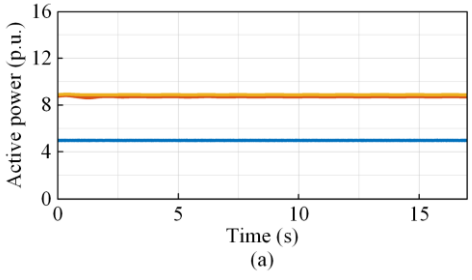

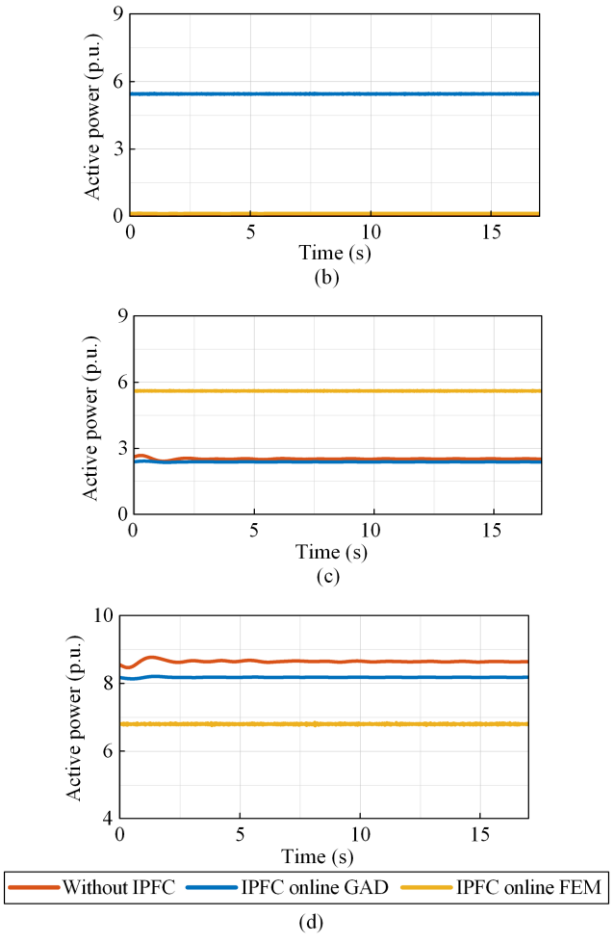

Fig. 7. Simulation results of active power in different lines in the steady state.

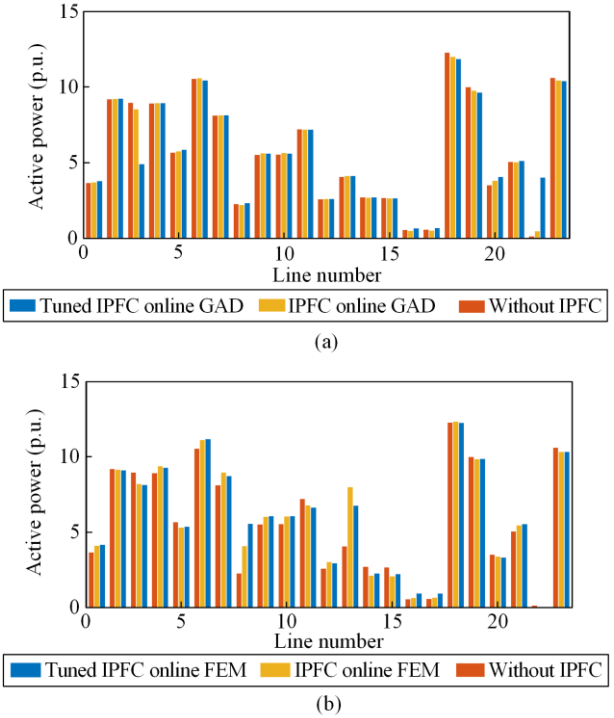

Fig. 8. Comparison of power flow before and after IPFC placed on different lines.

TABLE V
ACTIVE POWER OF LINES WITH AND WITHOUT IPFC AT STEADY STATE

Line	Active power (p.u.)				
	Without IPFC	IPFC online GAD	Tuned IPFC online GAD	IPFC online FEM	Tuned IPFC online FEM
TAZ	−3.6702	−3.7194	−3.8039	−4.1124	−4.1849
FED	9.2034	9.2302	9.2571	9.1571	9.1119
GAD	8.9661	8.5437	4.9188	8.2185	8.1528
DOF	8.9232	8.9443	8.9531	9.3961	9.2877
BES	5.6832	5.7665	5.8615	5.3287	5.3908
MAW	10.5678	10.5945	10.4502	11.1302	11.1817
SHD	8.1249	8.1568	8.1393	8.9758	8.7500
FEM	2.2664	2.2176	2.3487	4.0911	5.5823
XIM	5.5301	5.6288	5.6051	6.0401	6.0693
JIS	5.5494	5.6484	5.6247	6.0605	6.0897
NAH	7.2162	7.1952	7.2072	6.8022	6.6514
FUP	−2.5895	−2.6097	−2.6163	−3.0400	−2.9440
FEY	4.0808	4.1353	4.1460	8.0051	6.7855
SHS	2.7253	2.7019	2.7166	2.1373	2.2698
SHP	2.6722	2.6492	2.6636	2.0957	2.2256
XID	−0.5585	−0.5117	−0.6745	0.6590	0.9397
DOT	0.5786	0.5309	0.6970	-0.6623	−0.9481
SHW	12.2913	12.0195	11.8712	12.3502	12.2780
XIS	−10.0011	−9.7855	−9.6577	−9.8524	−9.8852
GAJ	3.5167	3.8145	4.0653	3.3924	3.3321
WUC	−5.0547	−5.0533	−5.1373	−5.4676	−5.5442
YIJ	0.1455	0.4838	4.0334	0.0086	0.0215
CHL	10.6111	10.4451	10.4195	10.3568	10.3561

2) N-1 Fault Scenario

The *N*-1 fault is a safety criterion in modern power systems, and so the performance of the IPFC during an *N*-1 fault is also of great importance. Following a line disconnection, there is a shift in power flow and voltage drop, which can lead to line overload and a decline in power supply quality. A three-phase short circuit is triggered at 5 s and lasts for 120 ms to simulate the fault. Figure 9 illustrates the PFDEI curves of the IPFC with different control instructions in the event of an *N*-1 fault after the IPFC is placed on lines GAD and FEM. Without IPFC, the PFDEI of the system is 1.2895. When the IPFC is placed on lines GAD and FEM, the system's PFDEI reaches minimum values of 1.2621 and 1.2828, respectively. This represents a decrease of 0.0274 and 0.0067, respectively, compared to the system without

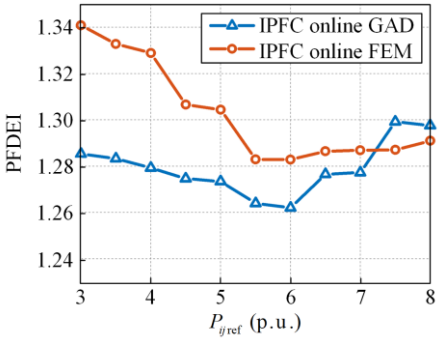

Fig. 9. The PFDEI of different lines with an *N*-1 fault.

IPFC. Placing the IPFC on line GAD results in a lower overall PFDEI level than placing it on line FEM. The control instructions for the IPFC, when the PFDEI is minimum, are shown in Table VI.

TABLE VI
OPTIMAL IPFC INSTRUCTIONS UNDER THE *N*-1 FAULT

IPFC location	$P_{ij\,\mathrm{ref}}$ (p.u.)	$Q_{ij\,\mathrm{ref}}$ (p.u.)	$Q_{ik\,\mathrm{ref}}$ (p.u.)	PFDEI
GAD	6	2.5	0.51	1.2621
FEM	6	1.05	0.33	1.2630

The simulation curves of the output power of the tuned IPFC following the optimal instruction under the *N*-1 fault are shown in Fig. 10. The power of some other lines in different conditions is shown in Table VII. Because of the influence of power flow transfer, although the IPFC can control the power of the main line, the PFDEI value during the *N*-1 fault is still higher than the value in steady state. However, as the IPFC controls the power of the line with the greatest impact on power flow transfer to an acceptable range, while other lines share the overload part of the power flow. Therefore the possibility of line overload and cascade accidents caused by an *N*-1 fault in the system is reduced when the IPFC is placed on line GAD, compared to either without IPFC or when the IPFC is placed at other locations. After the *N*-1 fault, a significant portion of the power previously flowing from the disconnected line is redirected to line GAD, and the power flows of other lines also change to some extent.

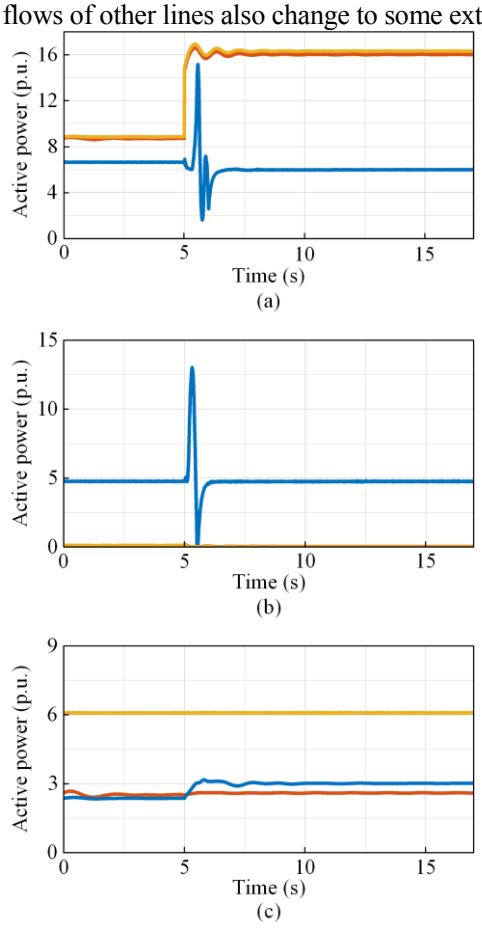

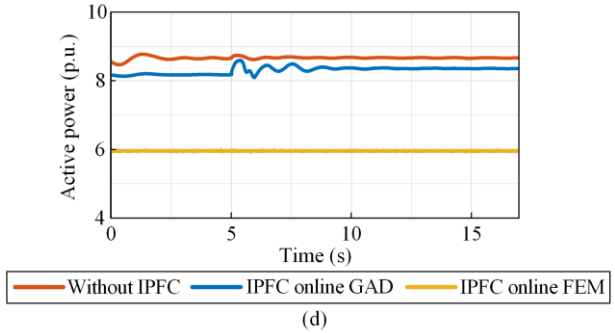

Fig. 10. Simulation results of active power in different lines with the *N*-1 fault.

TABLE VII
ACTIVE POWER OF LINES WITH AND WITHOUT IPFC IN STEADY STATE

Line	Active power (p.u.)				
	Without IPFC	IPFC online GAD	Tuned IPFC online GAD	IPFC online FEM	Tuned IPFC online FEM
TAZ	−3.5640	5.2301	5.6138	4.1638	4.2256
FED	7.8599	9.9095	9.7722	9.1937	9.2431
GAD	15.9826	8.4183	6.0011	15.3406	15.1755
DOF	10.7794	8.8495	8.7585	9.2620	9.1144
BES	6.2900	3.8881	4.2669	5.3239	5.2628
MAW	12.3124	10.2514	10.1450	10.8943	10.9490
SHD	4.2323	8.2044	8.1555	8.6977	9.0219
FEM	2.5847	2.3180	2.4558	3.9212	6.0011
XIM	4.0777	8.1546	4.0937	0.2541	6.2216
JIS	7.1355	5.1903	5.2929	5.8707	5.9041
NAH	5.0513	7.1721	7.2053	6.8417	6.6263
FUP	−4.3536	−2.4493	−2.5327	−2.9208	−2.7897
FEY	4.3478	4.0777	4.0937	8.1546	6.2216
SHS	0.3511	2.6968	2.7413	2.3188	2.1284
SHP	0.3456	2.6442	2.6878	2.2737	2.0871
XID	−2.6509	−0.7370	-0.8866	−0.3759	−0.7521
DOT	2.7179	0.7608	0.9135	0.3734	0.7567
SHW	11.9939	16.5885	15.5462	12.6015	12.6381
XIS	−9.8207	−13.3518	−12.5259	−10.1706	−10.1758
GAJ	3.1957	0.1491	1.2296	2.9110	2.8360
WUC	−4.8759	−6.5732	−6.9526	−5.5003	−5.5607
YIJ	0.0465	1.8305	3.7998	0.1080	0.1245
CHL	10.5275	13.0268	12.4065	10.6209	10.5926

Figures 11 and 12 compare the power flow distribution and bus voltages in the *N*-1 fault condition. The impact of power flow shifts resulting from line breakage on other lines is mitigated to varying degrees under the control of the IPFC. The most notable effect is seen on line GAD, where the active power is reduced from 1598 MW (without IPFC) to 600 MW and the fault node voltage is increased from 0.9263 to 0.9495 after the installation of the IPFC. The voltage stability of the fault bus node has significantly improved on line GAD compared to line FEM. With the tuned IPFC on line GAD, the active power of line 18 decreases from 1554 MW to 1200 MW, while the transmission power

of line 22 increases from 5 MW to 380 MW. With the tuned IPFC on line FEM, the active power of line 8 increases from 258 MW to 600 MW. Similar to the steady-state case, the degree of change before and after tuning the IPFC varies across different lines. While the IPFC, through its parallel converters, can control the operational states of multiple lines simultaneously, its regulatory capabilities are somewhat limited relative to expansive, mature modern power systems. Consequently, its performance manifests differently across various lines. Generally, the installation location optimized by the proposed method, i.e., line GAD, results in a more reasonable range of the line load ratio. When *N*-1 faults cause power flow transfer, the line can still transmit power normally and the system flow distribution remains at a more uniform level.

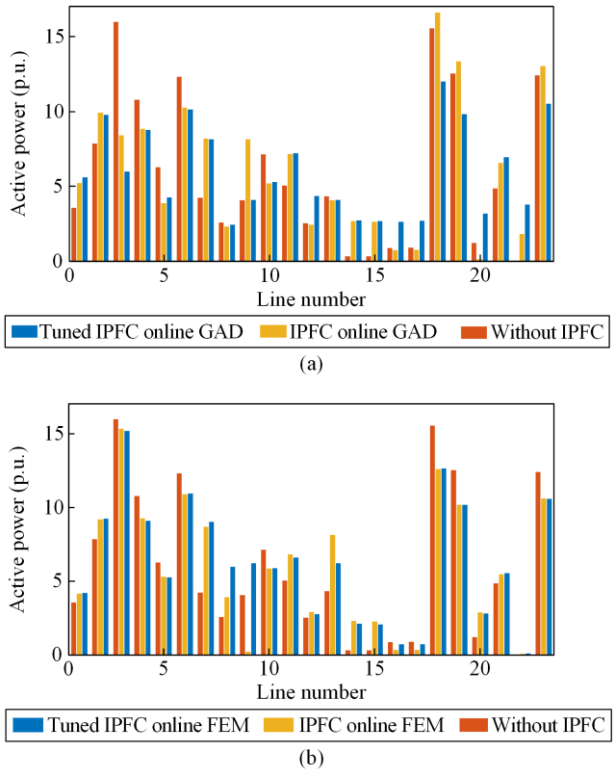

Fig. 11. Comparison of power flow before and after IPFC placed on different lines.

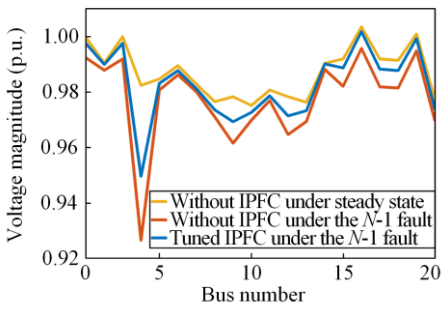

Fig. 12. Comparison of voltage magnitude before and after IPFC placed on line GAD.

VI. Conclusions

This paper addresses the issue of lack of consideration of power flow distribution in the existing IPFC placement method. It proposes the use of an entropy theory-based power flow transfer entropy index and power flow distribution entropy index for the IPFC placement method. The IPFC power control loop based on an MMC is analyzed, and an IPFC electromagnetic model is constructed in the ADPSS simulation platform. A practical power grid with over 800 nodes is used for electromagnetic-mechanical hybrid transient simulation. Based on the studies, the following conclusions can be drawn.

The system power flow transfer entropy index is proposed as an indicator for IPFC location selection. By calculating the line power flow transfer entropy index, it can quickly identify the line with the highest load urgency in different system operating conditions, thereby determining the optimal IPFC installation location. The location and capacity determination process, combined with entropy theory, comprehensively considers the steady-state power flow distribution and power flow fluctuation after an *N*-1 fault. The decision-making process is simple and efficient, and the results are globally optimal.

The system power flow distribution entropy index can effectively reflect the distribution of load rates among system lines. For the power system, appropriate IPFC control instructions can adjust the system's power flow distribution, so as to maximize power flow balance within a suitable range. This helps alleviate the overload pressure on heavily loaded lines and improves the utilization of other lines, thus enhancing system resilience to random disturbances.

The proposed IPFC configuration method, considering both the power flow transfer entropy index and the distribution index, provides a sound basis for determining the IPFC installation location and control instructions. For critical lines, it reduces the risk of overloading, improves voltage stability, and enhances the system's ability to resist disturbance factors. In the event of an *N*-1 fault, it limits line power fluctuation and reduces line power oscillation time. This approach not only improves the power flow distribution and balance, and line utilization rate in the steady state but also better handles random and uncertain disturbances. Therefore it can enhance transient stability during *N*-1 fault conditions and reduce the risk of cascading failures.

The proposed method in this paper has not taken into account factors like installation costs and system power losses. In future work, combining intelligent algorithms could enhance the completeness of IPFC placement and configuration. Additionally, as power systems are increasingly characterized by a high proportion of renewable energy sources and power electronic devices, the next research steps involve maintaining the key dynamic characteristics of the IPFC while simplifying

simulation models. Enhancing the transmission capacity of emerging power systems and achieving balanced line flow distribution will be the focus.

ACKNOWLEDGEMENT

Not applicable.

AUTHOR CONTRIBUTIONS

Qiuyu Li: the acquisition, analysis, and interpretation of data. Baohong Li and Qin Jiang: the conception and design of the work. Tianqi Liu, Yin Yue and Yingmin Zhang: draft the manuscript and substantively revise it. All authors read and approved the final manuscript.

FUNDING

This work is supported by the Natural Science Foundation of Sichuan Province of China (No. 2022NSFSC0262) and the Fundamental Research Funds for the Central Universities (No. 2022SCU12005).

AVAILABILITY OF DATA AND MATERIALS

Not applicable.

DECLARATIONS

Competing interests: The authors declare that they have no known competing financial interests or personal relationships that could have appeared to influence the work reported in this article.

AUTHORS' INFORMATION

Qiuyu Li received the B.S. degree from the College of Electrical Engineering and Information Technology, Sichuan University, Chengdu, China, in 2022. She is currently working toward to the M.S. degrees in Sichuan University. Her research interests include power system stability analysis and control and FACTS.

Baohong Li received the B.S., M.S., and Ph.D. degrees from the College of Electrical Engineering and Information Technology, Sichuan University, Chengdu, China, in 2009, 2015, and 2018. From 2009 to 2012, he was with State Grid Corporation of China. From 2019 to 2020, he has been a visiting scholar with Aalborg University, Aalborg, Denmark. He is currently an associate professor with the College of Electrical Engineering, Sichuan University. His research interests include power system stability analysis and control, high-voltage direct current transmission technologies, and DC grids.

Qin Jiang received the B.S. and Ph.D. degrees from the College of Electrical Engineering, Sichuan University, Chengdu, China, in 2016 and 2021, respectively. She is currently a lecturer with the College of Electrical Engineering, Sichuan University. Her research interests include power system stability analysis and control and high-voltage direct current transmission technologies.

Tianqi Liu received the B.S. and M.S. degrees from Sichuan University, Chengdu, China, in 1982 and 1986, respectively, and the Ph.D. degree from Chongqing University, Chongqing, China, in 1996, all in electrical engineering. She is currently a professor with the College of Electrical Engineering and Information Technology, Sichuan University. Her research interests include power system stability, HVDC, optimal generation dispatch, dynamic security analysis, dynamic state estimation, and load forecast.

Yue Yin received the B.S. degree from the School of Mechanical and Energy Engineering, Jimei University, Xiamen, China, in 2006, and the M.S. degree in control science and engineering and the Ph.D. degree in electrical engineering from Sichuan University, Chengdu, China, in 2010 and 2020, respectively. She is currently an associate professor with the College of Electrical Engineering, Sichuan University. Her research interests include stochastic optimization on power system operation and planning with renewable energy.

Yingmin Zhang received the M.S. and Ph.D. degrees in electrical engineering from Sichuan University, Chengdu, China, in 1998 and 2013, respectively. She is currently a full professor with the College of Electrical Engineering, Sichuan University. Her current research interests include stability analysis and control of modern power system, grid-integration of new energy systems, and HVDC transmission technology.

REFERENCES

[1] S. E. G. Mohamed, "Power flow control capability of the power transistor-assisted Sen transformer and the unified power flow controller: a close comparison," *IET Generation, Transmission & Distribution*, vol. 14, no. 15, pp. 3033-3041, Jun. 2020.

[2] R. Upputuri, N. Kumar, "Assessment and enhancement of static power system security with multi-line FACTS devices under congestion conditions," *International Transactions on Electrical Energy Systems*, vol. 31, no. 11, pp. 26-40, Nov. 2021.

[3] M. K. Kar, S. Kumar, and A. K. Singh *et al.*, "Reactive power management by using a modified differential evolution algorithm," *Optimal Control Applications and Methods*, vol. 44, no. 2, pp. 967-986, Mar. 2023.

[4] A. N. Khan, K. Imran, and M. Nadeem *et al.*, "Ensuring reliable operation of electricity grid by placement of FACTS devices for developing countries," *Energies*, vol. 14, no. 8, pp. 22836, Apr. 2021.

[5] Y. Sang, M. Sahraei-Ardakani, "Effective power flow control via distributed FACTS considering future uncertainties," *Electric Power Systems Research*, vol. 168, pp. 127-136, Mar. 2019.

[6] H. Tsai, J. Liu, and C. Chu, "Integrations of neural networks and transient energy functions for designing supplementary damping control of UPFC," *IEEE Transactions on Industry Applications*, vol. 55, no. 6, pp. 6438-6450, Nov. 2019.

[7] Z. Luburić, H. Pandžić, "FACTS devices and energy storage in unit commitment," *International Journal of Electrical Power & Energy Systems*, vol. 104, pp. 311-325, Jan. 2019.

[8] F. Massimo, D. Lauria, and S. Quaia *et al.*, "Analytical methods for series compensation of a transmission line," *International Journal of Electrical Power & Energy Systems*, vol. 145, Feb. 2023.

[9] S. Feng, X. Wu, and Z. Wang *et al.*, "Damping forced oscillations in power system via interline power flow controller with additional repetitive control," *Protection and Control of Modern Power Systems*, vol. 6, no. 2, pp. 264-275, Apr. 2021.

[10] A. Mishra, V. N. K. Gundavarapu, and V. R. Bathina *et al.*, "Real power performance index and line stability index-based management of contingency using firefly algorithm," *IET Generation, Transmission & Distribution*, vol. 10, no. 10, pp. 2327-2335, Jul. 2016.

[11] P. Singh, N. Senroy, R. Tiwari, "Guaranteed convergence embedded system for SSSC and IPFC," *IEEE Transactions on Power Systems*, vol. 36, no. 3, pp. 2725-2728, May 2021.

[12] M. L. Woldesemayat, A. T. Tantu, "Security enhancement of power systems through interline power flow controller (IPFC) under contingency condition: a case study and analysis-EEP 400 kV system," *Journal of Electrical and Computer Engineering*, Nov. 2022.

[13] B. Fardanesh, "Optimal utilization, sizing, and steady-state performance comparison of multiconverter VSC-based FACTS controllers," *IEEE Transactions on Power Delivery*, vol. 19, no. 3, pp. 1321-1327, Jul. 2004.

[14] N. K. Sharma, A. Ghosh, R. K. Varma, "A novel placement strategy for facts controllers," *IEEE Transactions on Power Delivery*, vol. 18, no. 3, pp. 982-987, Jul. 2003.

[15] X. Zhang, D. Shi, and Z. Wang *et al.*, "Optimal allocation of series FACTS devices under high penetration of wind power within a market environment," *IEEE Transactions on Power Systems*, vol. 33, no. 6, pp. 6206-6217, Nov. 2018.

[16] J. S. Pereira, E. A. Belati, and C. F. D. Nascimento *et al.*, "A mathematical programming approach for allocation and analysis of TCSC in power transmission system," *IEEE Latin America Transactions*, vol. 20, no. 7, pp. 2001-2009, Jul. 2022.

[17] S. Marrero-Vera, M. Hernandez-Tejera, and I. Nuez-Pestana *et al.*, "Pareto optimality for FACTS devices placement considering demand variations," *Electric Power Systems Research*, vol. 211, Oct. 2022.

[18] A. A. Ahmad, R. Sirjani, "Optimal placement and sizing of multi-type FACTS devices in power systems using metaheuristic optimisation techniques: an updated review," *Ain Shams Engineering Journal*, vol. 11, no. 3, pp. 611-628, Sep. 2020.

[19] Y. C. Chang, "Multi-objective optimal SVC installation for power system loading margin improvement," *IEEE Transactions on Power Systems*, vol. 27, no. 2, pp. 984-992, May 2012.

[20] A. Elmitwally, A. Eladl, "Planning of multi-type FACTS devices in restructured power systems with wind generation," *International Journal of Electrical Power & Energy Systems*, vol. 77, pp. 33-42, May 2016.

[21] S. R. Inkollu, V. R. Kota, "Optimal setting of FACTS devices for voltage stability improvement using PSO adaptive GSA hybrid algorithm," *Engineering Science and Technology, an International Journal*, vol. 19, no. 3, pp. 1166-1176, Sep. 2016.

[22] S. Ranganathan, M. S. Kalavathi, and C. A. Rajan, "Self-adaptive firefly algorithm based multi-objectives for multi-type FACTS placement," *IET Generation, Transmission & Distribution*, vol. 10, no. 11, pp. 2576-2584, Aug. 2016.

[23] S. J. Galloway, I. M. Elders, and G. M. Burt *et al*, "Optimal flexible alternative current transmission system device allocation under system fluctuations due to demand and renewable," *IET Generation, Transmission & Distribution*, vol. 4, pp. 725-735, Jun. 2010.

[24] A. A. bduljabbar and J. V. Milanović, "Assessment of techno-economic contribution of FACTS devices to power system operation," *Electric Power Systems Research*, vol. 80, no. 10, pp. 1247-1255, Aug. 2010.

[25] J. P. Roselyn, D. Devaraj, S. S. Dash, "Multi-objective genetic algorithm for voltage stability enhancement using rescheduling and FACTS devices," *Ain Shams Engineering Journal*, vol. 5, no. 3, pp. 789-801, Jul. 2014.

[26] S. P. Dash, K. R. Subhashini, J. K. Satapathy, "Optimal location and parametric settings of FACTS devices based on JAYA blended moth flame optimization for transmission loss minimization in power systems," *Microsystem Technologies*, vol. 26, no. 5, pp. 1543-1552, May 2020.

[27] S. Galvani, M. T. Hagh, and M. B. B. Sharifian *et al.*, "Multi-objective predictability-based optimal placement and parameters setting of UPFC in wind power included power systems," *IEEE Transactions on Industrial Informatics*, vol. 15, no. 2, pp. 878-888, Feb. 2019.

[28] V. Frolov, P. G. Thakurta, and S. Backhaus *et al.*, "Operations- and uncertainty-aware installation of FACTS devices in a large transmission system," *IEEE Transactions on Control of Network Systems*, vol. 6, no. 3, pp. 961-970, Sep. 2019.

[29] S. Rezaeian-Marjani, H. Ebrahimi, and B. Tousi, "Probabilistic multi-objective optimization method for interline power flow controller (IPFC) allocation in power systems," *IET Generation, Transmission & Distribution*, vol. 16, no. 24, pp. 4951-4962, Dec. 2022.

[30] A. Mishra, V. N. K. Gundavarapu, "Line utilisation factor-based optimal allocation of IPFC and sizing using firefly algorithm for congestion management," *IET Generation, Transmission & Distribution*, vol. 10, no. 1, pp. 115-122, Jan. 2016.

[31] Z. J. Bao, Y. J. Cao, and G. Z. Wang *et al.*, "Analysis of cascading failure in electric grid based on power flow entropy," *Physics Letters A*, vol. 373, no. 34, pp. 3032-3040, Aug. 2009.

[32] X. Gu, T. Liu, and S. Li *et al.*, "Identification of vulnerable nodes in power grids based on graph deep learning algorithm," *IET Generation, Transmission & Distribution*, vol. 17, no. 9, pp. 2015-2027, May 2023.

[33] B. Wang, H. Ma, and X. Wang *et al.*, "Vulnerability assessment method for cyber-physical system considering node heterogeneity," *The Journal of Supercomputing*, vol. 76, no. 4, pp. 2622-2642, Apr. 2020.